NANO LETTERS

2007
Vol. 7, No. 5
1282−1285

Mechanisms of Quantum Dot Energy Engineering by Metalorganic Vapor Phase Epitaxy on Patterned Nonplanar Substrates

E. Pelucchi,*,†,§ S. Watanabe,†,‖ K. Leifer,†,⊥ Q. Zhu,† B. Dwir,† P. De Los Rios,‡ and E. Kapon†

Ecole Polytechnique Fédérale de Lausanne (EPFL), Laboratory of Physics of Nanostructures, CH-1015 Lausanne, Switzerland, Ecole Polytechnique Fédérale de Lausanne (EPFL), Institute of Theoretical Physics, CH-1015 Lausanne, Switzerland

Received January 25, 2007; Revised Manuscript Received March 19, 2007

ABSTRACT

A novel technique for tuning the strength of quantum confinement in site-controlled semiconductor quantum dots (QDs) is introduced and investigated theoretically and experimentally. The method makes use of controlled local growth rates during metalorganic vapor phase epitaxy on patterned arrays of inverted pyramids. A model accounting for precursor migration and adatom incorporation predicts the tuning in QD thickness as a function of the pattern parameters. The results are in good agreement with experimental findings. This technique offers means for designing QD photonic structures with potential applications in QD-based cavity quantum electrodynamics and quantum information processing.

Site- and energy-controlled nanostructures are important for future electronic and optoelectronic applications as they will allow achieving controlled nanostructure position/density and predesigned quantized energy spectrum. For instance, site and emission energy control of quantum dots (QDs) is essential for optical microcavity and photonic crystal applications requiring precise positioning and resonant coupling of the dot(s) to given electromagnetic field modes.[1] While several QD preparation techniques, most notably colloidal growth[2] and Stranski−Krastanow (SK) epitaxy,[3] rely completely on spontaneous self-ordering of the nanostructures, important efforts are currently directed at achieving ordered nucleation of quantum nanostructures, e.g., by growing SK dots or nanowires/nanorods on substrates prepatterned lithographically.[4] More recently, there have been also increasing efforts in developing approaches for tuning the energy of the confined states of QDs, e.g., using postgrowth, rapid, or laser thermal annealing.[5]

Seeded metalorganic vapor phase epitaxy (MOVPE) of inverted pyramidal QDs on prepatterned semiconductor substrates[6] has been demonstrated to be a successful alternative to self-assembled SK growth when high optical quality, highly uniform, site-controlled ordered arrays of semiconductor QDs are desired.[7,8] Moreover, we recently reported the control of quantum confinement in isolated pyramidal QDs by using substrate patterns consisting of a single pyramid placed at the center of array "defects" free of pyramids. Strikingly, the emission wavelength of the isolated QD was blue-shifted with respect to that of the QD array; moreover, the wavelength could be tuned reproducibly by systematic variations in the array pattern.[9] These results suggested that the growth rate at the nucleation position of a given pyramidal QD can be controlled by the surrounding nonplanar pattern. However, a quantitative model accounting for this phenomenon has not been proposed so far.

In this paper, we present a growth model, which clarifies the mechanisms of local growth rate control of pyramidal QDs on patterned substrates. It is shown that metallorganic precursor migration and decomposition play a key role in determining the QD growth rate and hence thickness. The results of the model agree with experiments and allow

* Corresponding author. E-mail: emanuele.pelucchi@tyndall.ie.
† Ecole Polytechnique Fédérale de Lausanne (EPFL), Laboratory of Physics of Nanostructures.
‡ Ecole Polytechnique Fédérale de Lausanne (EPFL), Institute of Theoretical Physics.
§ Present address: Tyndall National Institute, "Lee Maltings", Prospect Row, Cork, Ireland.
‖ Present address: Department of Physics, Faculty of Science, University of Tokyo, 7-3-1 Hongo, Bunkyo-ku, Tokyo 113-0033, Japan.
⊥ Present address: Institute of Electron Microscopy and Nano Engineering Uppsala University, Angstromlaboratory, Lagerhyddsv. 1, 751 21 Uppsala, Sweden.

10.1021/nl0702012 CCC: $37.00
Published on Web 03/31/2007

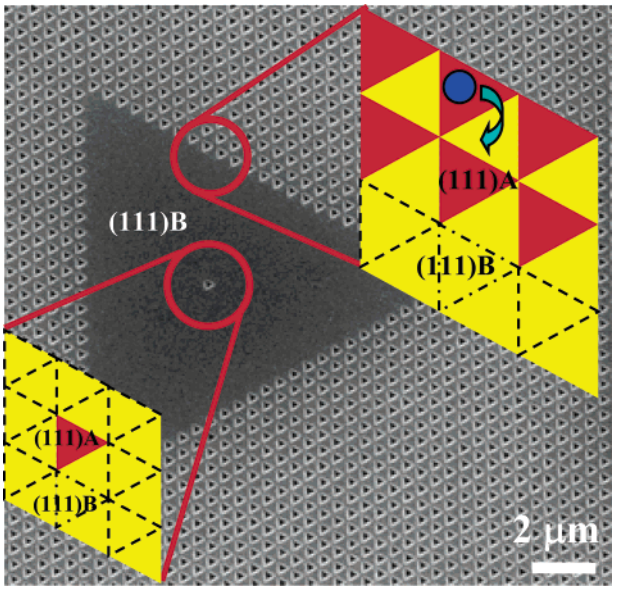

Figure 1. Scanning electron microscopy image of a representative (500 nm pitch) triangular sample patterning geometry. The schematic drawings show the triangular tiling of (111)A and (111)B zones used in the model.

designing the confinement energy of a QD placed at a desired position on the substrate.

The pyramidal QD structures were grown by low pressure (20 mbar) MOVPE on 2° off-(111)B GaAs substrates patterned with arrays of inverted tetrahedral pyramids exposing (111)A facets.[9] Arrays of different configurations were prepared using electron beam lithography, and wet chemical etching as described in detail in ref 9. The grown heterostructure consisted of a GaAs or $In_{0.10}Ga_{0.90}As$ QD layer sandwiched between $Al_{0.30}Ga_{0.70}As$ barrier layers, all nominally undoped. The growth was carried out in nitrogen carrier gas with trimethylGa/In/Al as group III precursors and AsH_3 as group V precursor, with a V/III ratio of 800, estimated substrate temperature of ~700 °C, and nominal growth rates (measured on (100) GaAs substrates) of ~0.03 and 0.05 nm/s for the dot and barrier layers, respectively.[9] The lower AlGaAs layer thickness was designed such that the QD layer was deposited on a self-limiting surface profile of the inverted pyramid.[6] Low-temperature (10 K) cathodoluminescence (CL) or microphotoluminescence (μPL) spectroscopy was used to characterize the emission wavelengths of the QDs self-formed at the center of each pyramid, from which the dot thickness was inferred.

A typical array pattern studied is shown in Figure 1. A single tetrahedral pyramid is situated at the center of a triangular area free of pyramids, surrounded by a regular, triangular-lattice array of tetrahedral pyramids.[9] To model the growth process, we subdivide the patterned area into identical unit elements consisting of equilateral triangles overlapping *either* the (111)B unetched parts between pyramids or the projections of the (111)A pyramidal facets on the (111)B plane. The unpatterned (111)B regions (with no pyramids) are subdivided into similar triangles (see Figure 1). In summary, in our model, the unit elements are either A or B type, exchange group III precursors or adatoms and bear chemical properties of the (111)A or the (111)B GaAs surface with respect to precursor decomposition and incorporation rates. Growth is initiated by the arrival of trimethyl-III precursors at the substrate, after diffusion through a gas-phase boundary layer, at a rate of λ (per unit time and per element).[10] These species are adsorbed on the (111)A and (111)B surfaces (cells), followed by migration of the "adspecies" (or their fragments) on the surfaces via hopping between adjacent cells. The precursors can decompose (i.e., release group III adatoms) within each triangular cell j at a rate a_{dj} (or probability $p_{dj} = a_{dj}\Delta t$ in a period Δt). The adatoms can also diffuse on the surfaces via an analogous hopping mechanism, with a probability p_{ai} of attaching and being incorporated into the semiconductor surfaces. The number of so-deposited adatoms in the (111)A cells defines the QD thicknesses.

Denoting the number of *nondecomposed* precursors inside cell i at a certain instant t by $n_i(t)$, we find at steady state

$$\rho_i - \sum_{j(nni)} {}^1/_3(1 - p_{dj})\rho_j = 1$$

where $\rho_j = n_j/\lambda\Delta t$ and the summation is limited to the three nearest neighbors.[11] The product of ρ_i and p_{di} yields the steady-state distribution of the deposited adatoms within the cells. The rate of incorporation is derived by considering Π_i, the steady-state distribution of unattached atoms, which is governed by the set of analogous equations

$$\Pi_i - \sum_{j(nni)} {}^1/_3(1 - p_{aj})\Pi_j = \rho_i p_{di}$$

This rate, multiplied by p_{ai}, gives the steady-state distribution of attached atoms per cell. The QD thickness is assumed to be proportional to $p_{ai}\Pi_i$. These sets of equations were solved numerically, employing arrays of 166 × 166 unit elements to minimize boundary effects. The decomposition rate of growth precursors on the planar (111)B surfaces was considered negligible compared to decomposition on (111)A planes, which is supported by the observation of very long (~40−60 μm) diffusion lengths of such precursors on the (111)B planes.[9]

We applied our model to 500 nm pitch, pyramidal GaAs QD arrays with triangular defects whose sides lengths were S = 13, 19, 28, or 34 unit elements. The ground state emission energies of the isolated QD placed at the center of the array defect, measured from low-temperature CL spectra, are higher than those of the array QDs and decrease monotonically with increasing triangle side (see Figure 2, diamonds). This reflects a systematic change in the QD thickness induced by the change in array pattern. Using transmission electron microscopy, cross-sectional atomic force microscopy, and luminescence data on similar structures, we modeled the QD transition energies as a function of the pyramidal QD thickness.[12] The relative variation in the QD thickness, thus derived from the CL measurements, is shown by the open squares in Figure 2.

The filled circles in Figure 2 represent the best fit to the relative variation in QD thickness obtained from the CL data

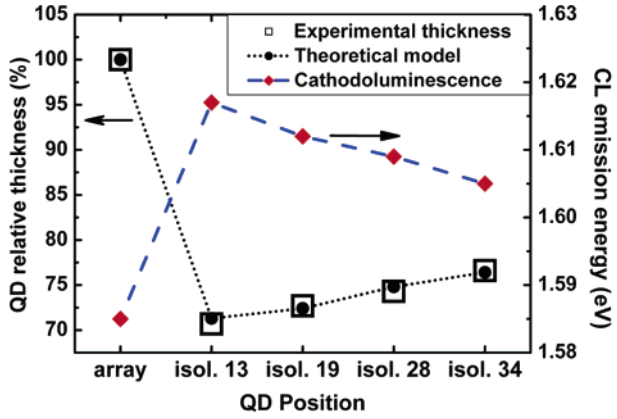

Figure 2. Right ordinate, diamonds: emission energy obtained from low-temperature cathodoluminescence (CL) spectra of QDs in the array (array QD) and isolated QDs inserted in a triangular defect pattern with 13, 19, 28, and 34 pyramid side ($S = 13$, 19, 28, and 34), i.e., 6, 9, 13.5, and 16.5 μm long. Left ordinate: ratio between thicknesses of isolated QD and array QD deduced from CL emission energy (open squares), and derived from best-fit of the growth model (circles). For graphics readability reasons, the open squares dimensions have been chosen so as to represent also the experimental error bar in the CL determination.

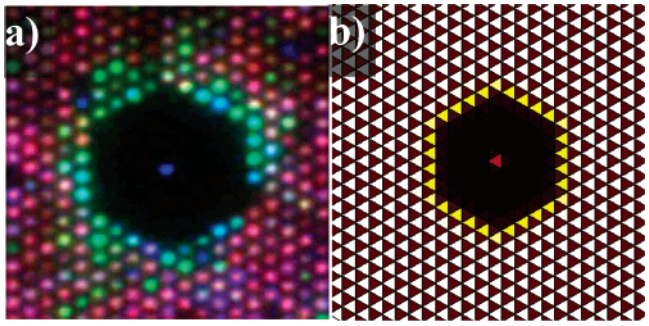

Figure 3. (a) False-color wavelength dispersive CL image of InGaAs QDs grown on a 500 nm pitch array with a hexagonal defect (reproduced from ref 9). (b) Simulation of the QD thickness distribution using the growth model as described in detail in the text. "Hotter" colors represent thicker QDs (see text).

analysis. This best fit was generated by varying the three free parameters of our growth model: the probability of precursors decomposition on (111)A planes $p_{di} = P_{dA}$ (assuming the probability of precursors decomposition on (111)B planes $p_{dj} = P_{dB} = 0$) and the probability for adatoms attachments on (111)A and on (111)B planes $p_{ai} = P_{aA}$ and $p_{aj} = P_{aB}$. The best fit was obtained with $P_{dA} = 0.0002$, $P_{aA} = 0.45$, and $P_{aA}/P_{aB} = 2$. With these fitting parameters, the growth model correctly predicts the blue-shift in the emission energy of the isolated dots with respect to the array and also reproduces the smaller red-shift observed for increasing side length.

We also applied the growth model to the case of $In_{0.1}Ga_{0.9}As$ pyramidal QDs grown in a hexagonal array defect (array pitch of 500 nm).[9] The wavelength-dispersive CL image of the structure is reproduced in Figure 3a, showing the blue-shifted emission of the isolated QD at the center of the defect. The growth model, using the same best-fit parameters used in Figure 2 and treating equally the Ga and the In precursors, again predicts well the trend of QD

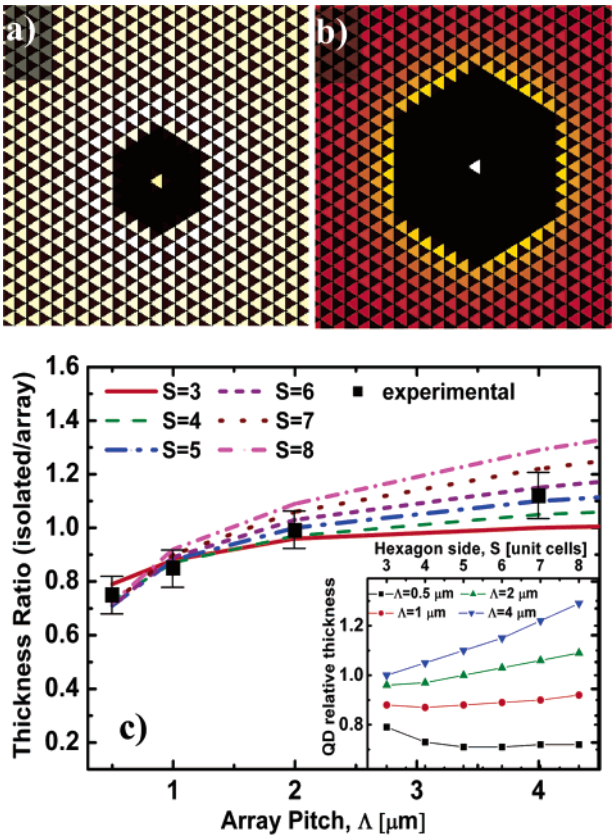

Figure 4. (a) Result of the simulation for a 2 micron pitch hexagonal defect with side $S = 5$. (b) Results of the simulation for a 4 micron pitch hexagonal defect with $S = 8$. (c) (Main) Calculated QD thickness ratio (isolated QD/array QD) dependence on array pitch Λ for different hexagon sides S (3−8 unit elements) and comparison with experiment (black squares). The experimental data reported refer to the following (S, pitch) configurations: (6, 0.5 μm), (5, 1 μm), (4−6, 2 μm), (8, 4 μm). (Inset) Same calculation results plotted as function of hexagon side S for the different array pitches we considered.

thickness variations observed experimentally (see Figure 3b). The growth model predicts an isolated InGaAs QD whose thickness is 71% of that of the array QDs, to be compared with the ~75% estimation based on the CL measurements. Moreover, the QDs arranged in the first ring surrounding the defect show an intermediate thickness between the array QD and the isolated QD. The thickness of the border QDs is predicted by the growth model to be ~92% of the thickness of the array QDs and ~90% of that thickness by the CL measurements. Similar differences in the QD thickness at the border of the defects were observed and simulated for the case of the triangular-defect structures of Figures 1 and 2. For example, in the sample with $S = 13$, the growth model predicts an average thickness of the border QDs of ~91% of the thickness of the array QDs, and the CL measurements yield an average value of ~87%.

The effect of changing the array pitch Λ (together with all other linear dimensions) on the QD thickness, for hexagonal array defects of different sides S, is presented in Figure 4 (main part). The calculated relative thickness, evaluated with parameters derived from the same best-fit model parameters as for Figures 2 and 3,[13] increases with

increasing array pitch. It also generally increases with defect size *S*, except for the smallest defects for the smaller pitches considered (see inset in Figure 4). The upper panel in Figure 4 shows the calculated thickness distributions for two selected structures. It can be seen that, for a certain range of pitch value ($\Lambda \approx 2\ \mu$m), the isolated QD has almost the same thickness as the array dots, whereas for still larger pitch values, it acquires a *larger* thickness than the array QDs. The relative QD thicknesses of (In)GaAs pyramidal QDs grown on several of these configurations, derived from low temperature μPL spectra as discussed above and shown by the filled circles in Figure 4, are in good agreement with the growth model.

The dependence of the QD growth rates on the pattern configuration can be interpreted by considering the preferential precursor decomposition on the (111)A facets and the subsequent diffusion of the product adatoms into the (111)B facets. To estimate the adatom diffusion length, we simulated the adatom distribution starting with precursors located in a single (111)A cell surrounded by a regular array (no defect). Using the best-fit parameters $P_{aA} = 0.45$ and $P_{dA} = 0.0002$, we estimated from the decay in deposition rates with distance from the source cell a diffusion length of $\sim$250 nm[14] for the Ga adatoms and $\sim 3\ \mu$m for the precursors. Thus, for a 500 nm pitch array, diffusion of adatoms from the isolated pyramid to the surrounding (111)B defect plan yields thinner isolated QD. As the defect size grows, the probability of readsorption of out-diffused adatoms increases, giving rise to thickening of the QD. For larger array pitch, the probability of out-diffusion from the isolated pyramid reduces and the readsorption rate augments, reversing the effect of QD thinning. We note that failing to account for precursor preferential decomposition and considering only surface diffusion and no-growth (111)B planes would invariably lead to *increased* thickness of the isolated QD due to in-diffusion into the isolated pyramid, in disagreement with experiment.

In conclusion, we have shown that by properly accounting for both precursor decomposition and adatom diffusion, it is possible to explain the controlled thickness variations observed in pyramidal QDs made by MOVPE on patterned (111)B substrates. Experimental results obtained for (In)GaAs/AlGaAs pyramidal QDs made on various pattern configurations are in good agreement with the presented growth model. Such ordered QDs with controlled emission energy should find applications in wavelength-selective optoelectronic devices such as multiwavelength lasers and single-photon emitters.

Acknowledgment. We acknowledge helpful discussions with F. Michelini.

References

(1) Badolato, A.; Hennessy, K.; Atatüre, M.; Dreiser, J.; Hu, E.; Petroff, P. M.; Imamoglu, A. *Science* **2005**, *308*, 1158. Hennessy, K.; Badolato, K.; Winger, M.; Gerace, D.; Atatüre, M.; Gulde, S.; Fält, S.; Hu, E. L.; Imamoğlu A. *Nature* **2007**, *445*, 896.
(2) Li, L. S.; Alivisatos, A. P. *Adv. Mater.* **2003**, *15*, 408.
(3) Springholz, G.; Holy, V.; Pinczolits, M.; Bauer, G. *Science* **1998**, *282*, 734.
(4) Kiravittaya, S.; Rastelli, A.; Schmidt, O. G. *Appl. Phys. Lett.* **2006**, *88*, 043112.
(5) Rastelli, A.; Wang, L.; Ulhaq, A.; Horton, F.; Kiravittaya, S.; Schmidt, O. Oral presentation, 4th International Conference on Quantum Dots, May 1−5, 2006, Chamonix, France. Rastelli, A.; Ulhaq, A.; Kiravittaya, S.; Wang, L.; Zrenner, A.; Schmidt, O. G. *Appl. Phys. Lett.* **2007**, *90*, 073120.
(6) Hartmann, A.; Loubies, L.; Reinhardt, F.; Kapon, E. *Appl. Phys. Lett.* **1997**, *71*, 1314.
(7) Pelucchi, E.; Baier, M.; Ducommun, Y.; Watanabe, S.; Kapon, E. *Phys. Status Solidi B* **2003**, *238*, 233. Baier, M. H.; Watanabe, S.; Pelucchi, E.; Kapon, E. *Appl. Phys. Lett.* **2004**, *84*, 1943. Watanabe, S.; Pelucchi, E.; Dwir, B.; Baier, M.; Leifer, K.; Kapon, E. *Appl. Phys. Lett.* **2004**, *84*, 2907. Leifer, K. et al., submitted.
(8) Baier, M. H.; Pelucchi, E.; Kapon, E.; Varoutsis, S.; Gallart, M.; Robert-Philip, I.; Abram, I. *Appl. Phys. Lett.* **2004**, *84*, 648. Baier M.; Constantin C.; Pelucchi E.; Kapon E. *Appl. Phys. Lett.* **1967**, *84*, 2004. Baier, M. et al., unpublished.
(9) Pelucchi, E.; Watanabe, S.; Leifer, K.; Dwir, B.; Kapon, E. *Physica E* **2004**, *23*, 476. Watanabe, S.; Pelucchi, E.; Leifer, K.; Malko, A.; Dwir, B.; Kapon, E. *Appl. Phys. Lett.* **2005**, *86*, 243105.
(10) That is to say, λ is the flux of precursors from the gas phase per unit element, so that $\lambda\Delta t$ are the precursors originated from the gas phase in the unit element during the interval Δt.
(11) Our set of equations are based on the following: we assume that the step Δt is long enough so that all the precursors previously present in a unit element at time t either decompose or out-diffuse from the element, which is justified by the extremely low growth rate we used. As a consequence, on average, we can treat the number of *nondecomposed* precursors in a unit element at a time $t + \Delta t$ as the result of the number of precursors deposited during the interval Δt plus those supplied by diffusion from the nearest neighbors, as any preexisting precursor will have either decomposed or outdiffused. The number of nondecomposed precursors at a certain instant t inside the element, $n_i(t)$, will then evolve in the time Δt according to $n_i(t + \Delta t) = \lambda\Delta t + \sum_{j(nni)} {}^1/_3(1 - a_{dj}\Delta t)n_j(t)$, where a_{dj} is the rate of precursor decomposition. The summation is limited only to nearest neighbor elements, with a coordination number of 3. In the steady state limit, where $n_i(t + \Delta t) \cong n_i$, and dividing by $\lambda\Delta t$, we will have $\rho_i - \sum_{j(nni)} {}^1/_3(1 - p_{dj})\rho_j = 1$, where $\rho_j = n_j/\lambda\Delta t$ and $p_{dj} = a_{dj}\Delta t$. We observe that, if the decomposition process has a relatively low probability, ρ_i is expected to be $\gg$1, being proportional to the nondecomposed n_i.
(12) Michelini, F.; Dupertuis, M.-A.; Kapon, E. *Appl. Phys. Lett.* **2004**, *84*, 4086. Michelini, F. et al., unpublished results.
(13) It can be shown that probabilities scale "exactly" with doubling the pattern pitch.
(14) Biasiol, G.; Kapon, E. *Phys. Rev. Lett.* **1998**, *81*, 2962.

NL0702012